La^{3+} Diffusion in the NASICON-Type Compound $La_{1/3}Zr_2(PO_4)_3$: X-ray Thermodiffraction, ^{31}P NMR, and Ionic Conductivity Investigations

M. Barré,*[,†,§] F. Le Berre,[†,§] M. P. Crosnier-Lopez,[†,§] O. Bohnké,[†,§] J. Emery,[‡,§] and J. L. Fourquet[†,§]

Laboratoire des Oxydes et Fluorures (UMR CNRS 6010), Laboratoire de Physique de l'Etat Condensé (UMR CNRS 6087), and Institut de Recherche en Ingénierie Moléculaire et Matériaux Fonctionnels (FR CNRS 2575), Université du Maine, Avenue Olivier Messiaen, 72085 Le Mans cedex 9, France

Received July 12, 2006. Revised Manuscript Received September 4, 2006

The NASICON-type compound $La_{1/3}Zr_2(PO_4)_3$ has been studied by thermal X-ray diffraction. It was found to exhibit, around 1000 °C, a reversible phase transition from $P\bar{3}$ to $P\bar{3}c1$ due to a modification of the lanthanum distribution in the $[Zr_2(PO_4)_3]^-$ network. This evolution was confirmed by ^{31}P NMR experiments performed on quenched $La_{1/3}Zr_2(PO_4)_3$ samples ($T = 700$ and 1000 °C) and compared to room-temperature results. To complete this study, impedance spectroscopy measurements were carried out between 330 and 730 °C, confirming the La^{3+} mobility in the NASICON network.

Introduction

$La_{1/3}Zr_2(PO_4)_3$ belongs to the NASICON family of general formula $A_xM_2(XO_4)_3$.[1] The structure consists of a three-dimensional network built from MO_6 octahedra and XO_4 tetrahedra interconnected by oxygen atoms.[2] The flexibility in these structures allows chemical substitutions, giving rise to a large number of isostructural phases.[3−5] Among this materials family, the $RE_{1/3}Zr_2(PO_4)_3$ series was first pointed out by Alami Talbi et al.[6] in 1994. More recently, these compounds were found to be RE^{3+} ionic conductors[7,8] and potential hosts for actinide immobilization,[9] whereas no structural study was undertaken until we published the room-temperature crystal structure of $La_{1/3}Zr_2(PO_4)_3$.[10] This compound crystallizes in the $P\bar{3}$ space group, a new one in the NASICON family. In a very recent paper[11] Bykov et al. indexed all the other $RE_{1/3}Zr_2(PO_4)_3$ diffraction patterns in the $P\bar{3}c1$ space group and confirmed the different behavior of the lanthanum variety. At the same time, a TEM investigation of $La_{1/3}Zr_2(PO_4)_3$ revealed the ability of La^{3+} ions to displace in the $[Zr_2(PO_4)_3]^-$ network.[12] To complete this work, we performed thermal X-ray diffraction, ^{31}P NMR spectroscopy, and ionic conductivity measurements on $La_{1/3}Zr_2(PO_4)_3$.

Experimental Section

Synthesis. $La_{1/3}Zr_2(PO_4)_3$ powder was synthesized from La_2O_3, $ZrOCl_2{\cdot}8H_2O$, and $NH_4H_2PO_4$ in stoichiometric ratios using a complex polymerizable method[13] as described in our previous paper.[10] The molar ratios employed for citric acid (CA) and ethylene glycol (EG) were respectively CA/M = 15/1 (M = [La] + [Zr]) and CA/EG = 1/4. The precursor obtained after the gel calcination at 350 °C was ground and a first annealing was performed in a furnace between 800 and 1000 °C. The powder obtained was then pelletized and heated at 1100 °C for 2 h. Three kinds of samples have been studied hereafter: the first one (A) was slowly cooled (rate of 100 °C/h with steps of 2 h every 50 °C) at 25 °C after annealing at 1100 °C while the two others were quenched from 700 °C (B) and 1000 °C (C) to room temperature in air, to retain the structures observed by thermal XRD at these temperatures.

Characterization. Thermal powder XRD measurements were recorded, on the slowly cooled sample (A), from 25 to 1000 °C in air, with Cu Kα radiation on a PANalytical X'Pert Pro diffractometer equipped with the X'celerator detector and an Anton Paar HTK 12 furnace. The details of data collections are presented in Table 1. Structure refinements were carried out by the Rietveld method, using Fullprof profile refinement software.[14] A pseudo-

* To whom correspondence should be addressed. E-mail: maud.barre.etu@univ-lemans.fr.
† Laboratoire des Oxydes et Fluorures.
§ Institut de Recherche en Ingénierie Moléculaire et Matériaux Fonctionnels.
‡ Laboratoire de Physique de l'Etat Condensé.

(1) Sljukic, M.; Matkovic, B.; Prodic, B.; Scavnicar, S. *Croat. Chem. Acta* **1967**, *39*, 145.
(2) Hagman, L. O.; Kierkegaard, P. *Acta Chem. Scand.* **1968**, *2*, 1822.
(3) Lightfoot, P.; Woodcock, D. A.; Jorgensen, J. D.; Short, S. *Int. J. Inorg. Mater.* **1999**, *1*, 53.
(4) Senbhagaraman, S.; Guru Row, T. N.; Umarji, A. M. *J. Mater. Chem.* **1993**, *3*, 309.
(5) El Jazouli, A.; El Bouari, A.; Fakrane, H.; Housni, A.; Lamire, M.; Mansouri, I.; Olazcuaga, R.; Le Flem, G. *J. Alloys Compd.* **1997**, *262*, 49.
(6) Alami Talbi, M.; Brochu, R.; Parent, C.; Rabardel, L.; Le Flem, G. *J. Solid State Chem.* **1994**, *110*, 350.
(7) Tamura, S.; Imanaka, N.; Adachi, G. *J. Alloys Compd.* **2001**, *323−324*, 540.
(8) Tamura, S.; Imanaka, N.; Adachi, G. *Solid State Ionics* **2002**, *154−155*, 767.
(9) Bois, L.; Guittet, M. J.; Carrot, F.; Trocellier, P.; Gauthier-Soyer, M. *J. Nucl. Mater.* **2001**, *297*, 129.
(10) Barré, M.; Crosnier-Lopez, M. P.; Le Berre, F.; Emery, J.; Suard, E.; Fourquet, J. L. *Chem. Mater.* **2005**, *17*, 6605.
(11) Bykov, D. M.; Gobechiya, E. R.; Kabalov, Y. K.; Orlova, A. I.; Tomilin, S. V. *J. Solid State Chem.* **2006**, *179*, 3101.
(12) Crosnier-Lopez, M. P.; Barré, M.; Le Berre, F.; Fourquet, J. L. *J. Solid State Chem.* **2006**, *179*, 2714.
(13) (a) Pechini, M. P. U.S. Patent 3330697, 1967. (b) Kakihana, M.; *J. Sol-Gel Sci. Technol.* **1996**, *6*, 7.
(14) Rodriguez-Carvajal, J. Program FULLPROF.2K, Version 3.20; Institut Laüe-Langevin: Grenoble, 2005.

10.1021/cm061610m CCC: $33.50
Published on Web 10/12/2006

Table 1. Condition of X-ray Data Collection for $La_{1/3}Zr_2(PO_4)_3$

diffractometer	Philips X'pert PRO
furnace	Anton Paar HTK12
radiation	X-ray Cu Kα
angular range/deg 2θ	5.00−110.00
step scan increment/deg 2θ	0.017
counting time	150 s step^{-1}
temperatures (°C)	25; 300; 500; 700; 1000

Table 2. NMR Experimental Conditions

parameters	1D experimental conditions
pulse length	3.57 μs
dead time	10 μs
recycle time	1000 s
resonance frequency	121.443 MHz
MAS spinning speed	10 kHz
number of scans	8
number of digitized points	1024
referencing 0 ppm	H_3PO_4 (85%)

Voigt function was applied for approximation of the diffraction profiles and background correction was made manually.

^{31}P NMR experiments were carried out at room temperature, on the three powdered samples. NMR spectra were recorded with a Bruker Avance (DSX) 300 spectrometer, working at $\nu_0 = 121.44$ MHz and using a 4 mm Magic Angle Spinning (MAS) probe spinning up to 15 kHz. The amplitude of the radio frequency field for ^{31}P is $\nu_1 = 70$ kHz. The experimental parameters are reported in Table 2. Owing to their long spin lattice relaxation times (up to 100 s) and to obtain quantitative results, the acquisition begins with a saturation sequence followed by a long recycle time delay (100 s) in the 1D experiment. DMFIT software[15] was used to fit the spectra and to obtain the line width, the peaks position, and the percentage of each contribution.

For electrical conductivity measurements, the sample A powder was uniaxially pressed into a pellet of diameter ≈5 mm and thickness ≈2.9 mm and then isostatically pressed at 400 MPa. The pellet was then sintered at 1000 °C for 4 h. The compaction obtained is only about 70% since the rapid decomposition of the phase does not allow sintering at a higher temperature or for a longer period of time. Measurements were carried out with ion-blocking sputtered Pt electrodes in a two-probe cell. The frequency response Analyser (Solartron 1260) and the Dielectric Interface (Solartron 1296) were used in the frequency domain from 10 MHz to 1 Hz. The measurements were performed in air and in dehydrated N_2 atmosphere, in the temperature range from 330 to 730 °C. Before any measurement, linearity and stationary of the electrochemical system were checked. So an ac voltage of 300 mV was used for every measurement and a waiting time of 45 min was necessary to obtain thermal equilibrium of the sample after each 50 °C step. Zview software of Solartron (version 2.6) based on the LEVM software of J. R. MacDonald was used for data refinement.

Results and Discussion

XRD Study. We recently published the room-temperature crystal structure of $La_{1/3}Zr_2(PO_4)_3$.[10] This phase crystallizes in $P\bar{3}$ space group with cell parameters ($a = 8.7492(2)$ Å; $c = 23.2483(5)$ Å; $Z = 6$) close to those of other NASICON-type compounds. In this study, the sample, synthesized by a complex polymerizable route, was heated at 1100 °C and naturally cooled to room temperature in the furnace. Rietveld refinements revealed an unusual distribution of the La^{3+} cation in the preserved $[Zr_2(PO_4)_3]^-$ NASICON network: 1 La^{3+} in the 1a (0,0,0) site (La1), 0.82(5) La^{3+} in the 1b (0,0,$^1/_2$) site (La2), and the remaining 0.18(3) La^{3+} in a 2d ($^1/_3$,$^2/_3$,0.6667) site (La3) (Figure 1a). Since this study, thermal X-ray diffraction measurements have been performed and have shown that the natural cooling did not allow the $La_{1/3}Zr_2(PO_4)_3$ phase to be obtained in the real thermal equilibrium state. Indeed, a XRD pattern recorded at room temperature for an extremely slow cooled sample presents subtle differences concerning the intensity of some peaks (003 and 101, for example) which are relative to the lanthanum repartition (Figure 2). A new Rietveld refinement has then been performed at room temperature, leading to a slightly different La^{3+} distribution: 1 La^{3+} in the La1 site, 0.56(1) in the La2 site, and the remaining 0.44(1) in the La3 one. Consequently, the following results correspond to the $La_{1/3}Zr_2(PO_4)_3$ slowly cooled compound (A) which can be considered at thermal equilibrium.

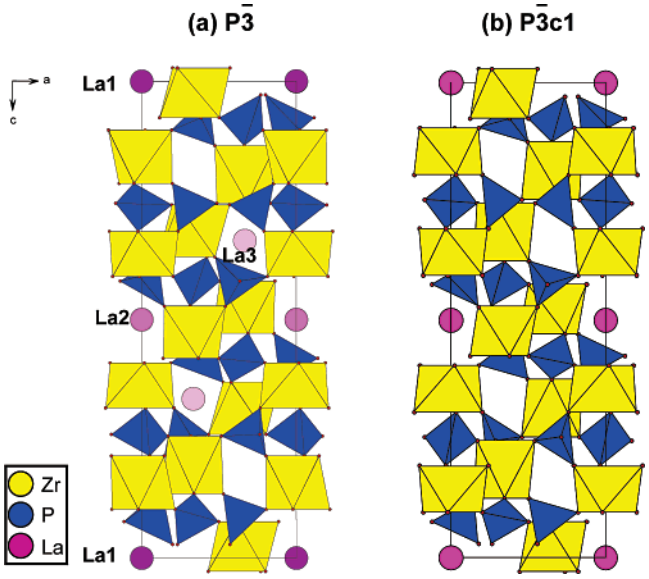

Figure 1. Evolution of $La_{1/3}Zr_2(PO_4)_3$ structure with temperature: (a) room temperature and (b) 1000 °C showing the La sites.

The thermal X-ray diffraction diagram evolution of sample A is represented in Figure 3. Below 500 °C, no significant modification is observed while above this temperature a

Table 3. Structure Refinements Results for $La_{1/3}Zr_2(PO_4)_3$ A Sample, at Room Temperature and 1000 °C

	RT	1000 °C
space group	$P\bar{3}$	$P\bar{3}c1$
number of refined parameters	102	78
peak shape, η	pseudo-Voigt 0.78(3)	pseudo-Voigt 0.50(1)
cell parameters/Å	$a = 8.7080(3)$ $c = 23.1710(1)$	$a = 8.7290(1)$ $c = 23.2201(4)$
half-width parameters	$u = 0.81(2)$ $v = -0.27(1)$ $w = 0.066(2)$ $x = -0.012(1)$	$u = 0.095(4)$ $v = -0.060(3)$ $w = 0.032(1)$ $x = -0.004(1)$
asymmetry parameters	$P_1 = -0.087(4)$ $P_2 = 0.002(1)$	$P_1 = -0.030(3)$ $P_2 = 0.007(1)$
R_{Bragg}	5.23%	3.27%
R_p	12.50%	8.86%
R_{wp}	11.40%	8.33%
R_{exp}	5.03%	4.62%
χ^2	5.15	3.24

(15) Massiot, D.; Fayon, F.; Capron, M.; King, I.; Le Calvé, S.; Alonso, B.; Durand, J.-O.; Bujoli, B.; Gan, Z.; Hoaston, G. *Magn. Reson. Chem.* **2002**, *40*, 70.

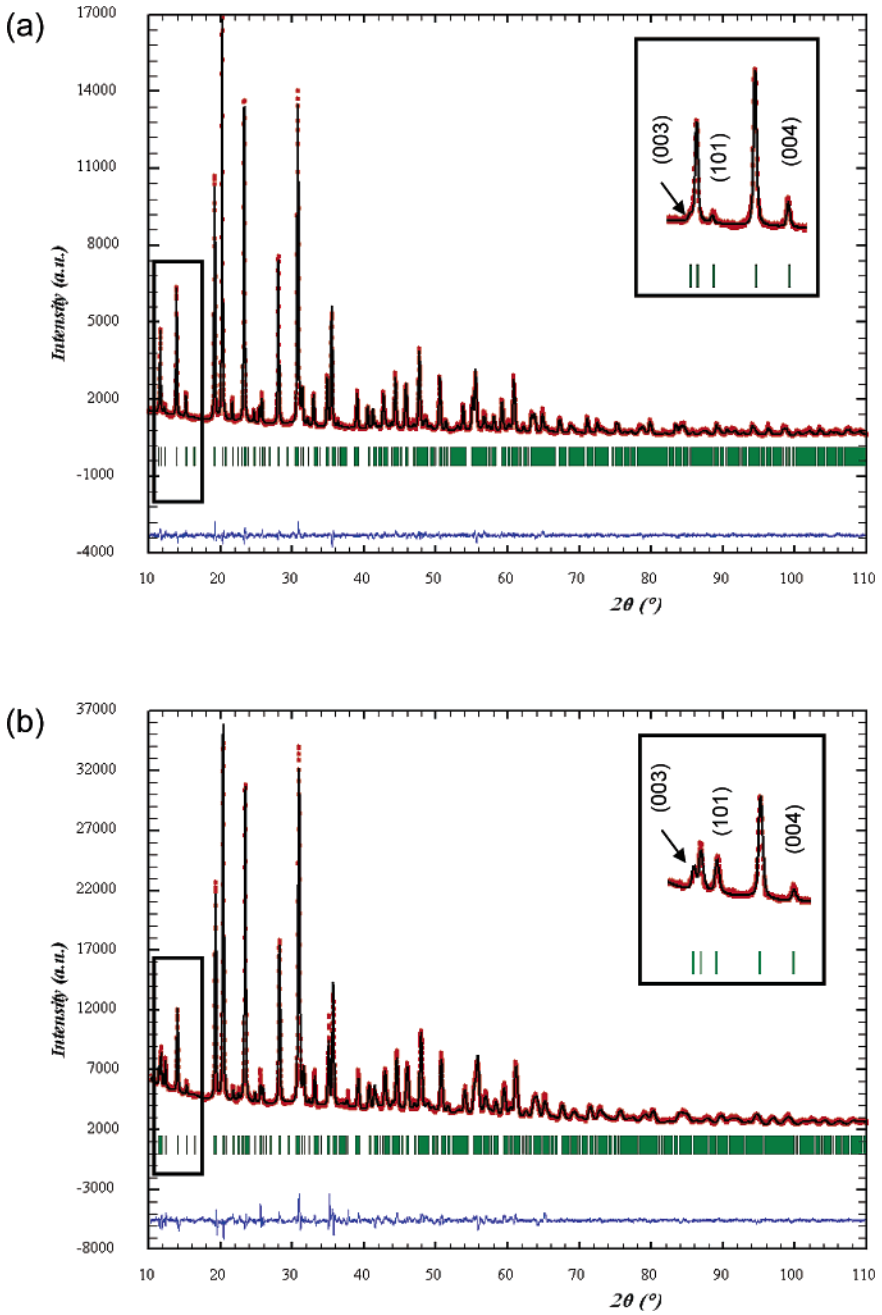

Figure 2. Room-temperature XRD pattern of $La_{1/3}Zr_2(PO_4)_3$: (a) natural cooling in the furnace; (b) extremely slow cooling controlled in the furnace (sample A).

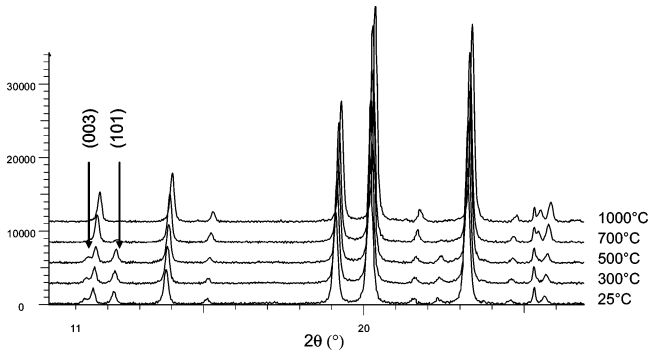

Figure 3. Part of X-ray thermodiffractograms of $La_{1/3}Zr_2(PO_4)_3$ (sample A) at low 2θ angle.

progressive diminution of the (003) and (101) diffraction peaks intensity occurs until complete disappearance around 1000 °C. Since the intensity of these peaks is directly linked to the La3 site population, we can deduce that temperature drives the lanthanum distribution in the $[Zr_2(PO_4)_3]^-$ network. This has been confirmed by Rietveld refinements (Table 3) at various temperatures which revealed that the La3 site progressively empties in favor of the La2 site. This phenomenon is clearly observed above 500 °C (Figure 4). At 1000 °C, this evolution finally leads to only two sites for La^{3+} ions, La1 and La2, which are then fully occupied. At this temperature the X-ray diffraction pattern can be correctly fitted with the more symmetrical $P\bar{3}c1$ space group; this fact indicates the occurrence of a structural phase transition $P\bar{3} \rightarrow P\bar{3}c1$ around 1000 °C (Figure 1b). This transition is reversible and presents a very large hysteresis. The refinement of thermal X-ray diffraction patterns show that, between

Table 4. Atomic Coordinates (RT and 1000 °C) for $La_{1/3}Zr_2(PO_4)_3$ Showing the $P\bar{3}$ to $P\bar{3}c1$ Transposition

	RT, $P\bar{3}$						1000 °C, $P\bar{3}c1$					
	site	s.o.f	*x*	*y*	*z*	*B* (10^{-2} Å^2)	site	s.o.f	*x*	*y*	*z*	*B* (10^{-2} Å^2)
Zr1	2c	1	0	0	0.1523(3)	0.67(8)	4c	1	0	0	0.1513(1)	0.85(2)
Zr2	2c	1	0	0	0.6469(3)	0.67(8)						
Zr3	2d	1	1/3	2/3	0.8106(3)	0.67(8)	4d	1	1/3	2/3	0.8123(1)	0.85(2)
Zr4	2d	1	1/3	2/3	0.3113(4)	0.67(8)						
Zr5	2d	1	1/3	2/3	0.5210(4)	0.67(8)	4d	1	1/3	2/3	0.5246(1)	0.85(2)
Zr6	2d	1	1/3	2/3	0.0214(4)	0.67(8)						
P1	6g	1	0.302(1)	0.008(1)	0.2563(3)	0.6(1)	6f	1	0.2880(8)	0	1/4	0.43(6)
P2	6g	1	0.957(1)	0.339(1)	0.5836(4)	0.6(1)	12g	1	0.9540(5)	0.3256(7)	0.5766(2)	0.43(6)
P3	6g	1	0.618(1)	0.679(1)	0.9224(3)	0.6(1)						
O1	6g	1	0.197(2)	0.051(3)	0.2135(8)	0.3(1)	12g	1	0.202(1)	0.961(1)	0.1937(3)	2.17(9)
O2	6g	1	0.027(4)	0.792(3)	0.6849(6)	0.3(1)						
O3	6g	1	0.854(4)	0.311(5)	0.5287(9)	0.3(1)	12g	1	0.825(1)	0.271(1)	0.5285(4)	2.17(9)
O4	6g	1	0.768(3)	0.199(4)	0.028(1)	0.3(1)						
O5	6g	1	0.526(4)	0.661(5)	0.8650(7)	0.3(1)	12g	1	0.503(1)	0.651(2)	0.8741(4)	2.17(9)
O6	6g	1	0.416(3)	0.524(4)	0.368(1)	0.3(1)						
O7	6g	1	0.197(2)	0.216(3)	0.103(1)	0.3(1)	12g	1	0.1848(9)	0.205(1)	0.0961(4)	2.17(9)
O8	6g	1	0.796(3)	0.815(1)	0.5909(9)	0.3(1)						
O9	6g	1	0.860(2)	0.499(3)	0.4189(7)	0.3(1)	12g	1	0.874(1)	0.498(1)	0.4229(5)	2.17(9)
O10	6g	1	0.501(2)	0.113(2)	0.9237(9)	0.3(1)						
O11	6g	1	0.514(2)	0.831(3)	0.7445(6)	0.3(1)	12g	1	0.539(1)	0.830(1)	0.7535(5)	2.17(9)
O12	6g	1	0.192(1)	0.434(2)	0.2583(9)	0.3(1)						
La1	1a	**1**	0	0	0	6.4(1)						
La2	1b	**0.56(1)**	0	0	0.5	6.4(1)	2b	**1**	0	0	0	7.5(1)
La3	2d	**0.22(1)**	1/3	2/3	0.666(3)	6.4(1)						

room temperature and 1000 °C, the *a* and *c* parameters increase from 8.7080 to 8.7290 Å and from 23.1710 to 23.2201 Å, respectively. These variations lead to the following expansion coefficients: $\alpha_a = 2.47 \times 10^{-6}$ °C^{-1} and $\alpha_c = 2.17 \times 10^{-6}$ °C^{-1} with a mean expansion coefficient of 2.37×10^{-6} °C^{-1}, in good agreement with the low thermal expansion usually encountered for these materials.[6,16,17]

Table 4 presents the final atomic parameters and B_{iso} values obtained by Rietveld refinement from both room temperature and 1000 °C data. We can note that atomic positions in $P\bar{3}c1$ can directly be transposed from the $P\bar{3}$ space group, clearly indicating that the $[Zr_2(PO_4)_3]^-$ skeleton remains unchanged and that the symmetry evolution is only due to the lanthanum distribution. All these results are consistent with those obtained from TEM study we recently published.[12] Indeed, in this work we observed a fast structural transition from $P\bar{3}$ to $P\bar{3}c1$ induced by the electron beam energy without any atomic contents modification. This transition is quickly followed by a new one, leading to a *R*--- extinction symbol. Until now, we did not succeed in producing this last R form out of the microscope due to the decomposition of the sample in temperature. This two-step transition $P\bar{3} \rightarrow P\bar{3}c1 \rightarrow$ R--- has been explained by the ability of La^{3+} to displace in the NASICON network. This is in agreement with the high B_{iso} value obtained by X-ray refinements and with the low bond valence values calculated for La^{3+} cations.

^{31}P NMR Study. The MAS 1D spectra performed at room temperature on $La_{1/3}Zr_2(PO_4)_3$ samples quenched at 700 °C (B) and 1000 °C (C) are presented in Figure 5 with the one obtained at room temperature (A). To account for all these spectra, we need five lines that we attributed to five chemically different phosphorus sites (Table 5). These five P sites had already been observed in the previous RMN study[10] (1D (MAS) and 2D) which evidenced that three phosphorus atoms (P1, P2, P3) were intercorrelated, meaning that they belong to the same homogeneous phase, while the other atoms (P4 and P5) were uncorrelated. This revealed that the sample was in fact constituted by two kinds of domains: one corresponding to the perfect ordering of La^{3+} ions on La1 (1a) and La2 (1b) sites, and the other, with a very small size owing to the lack of correlation, showing some extra La^{3+} ions distributed on the La3 (2d) position. We can note in Figure 5 a progressive vanishing of the P4 and P5 peaks as temperature changes. This means that the second domain narrows with temperature which is in agreement with thermal XRD results, confirming a La^{3+} displacement from La3 to La2 site. For the sample quenched at 1000 °C, we still observe the P4 and P5 contributions

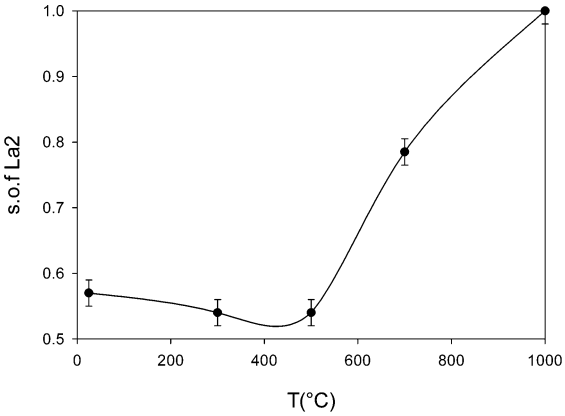

Figure 4. Variation versus temperature of La2 site (1b) occupation.

(16) Senbhagaraman, S.; Umarji, A. M. *J. Solid State Chem.* **1990**, *85*, 169.
(17) Woodcock, D. A.; Lightfoot, P.; Smith, R. I. *J. Mater. Chem.* **1999**, *9*, 2631.

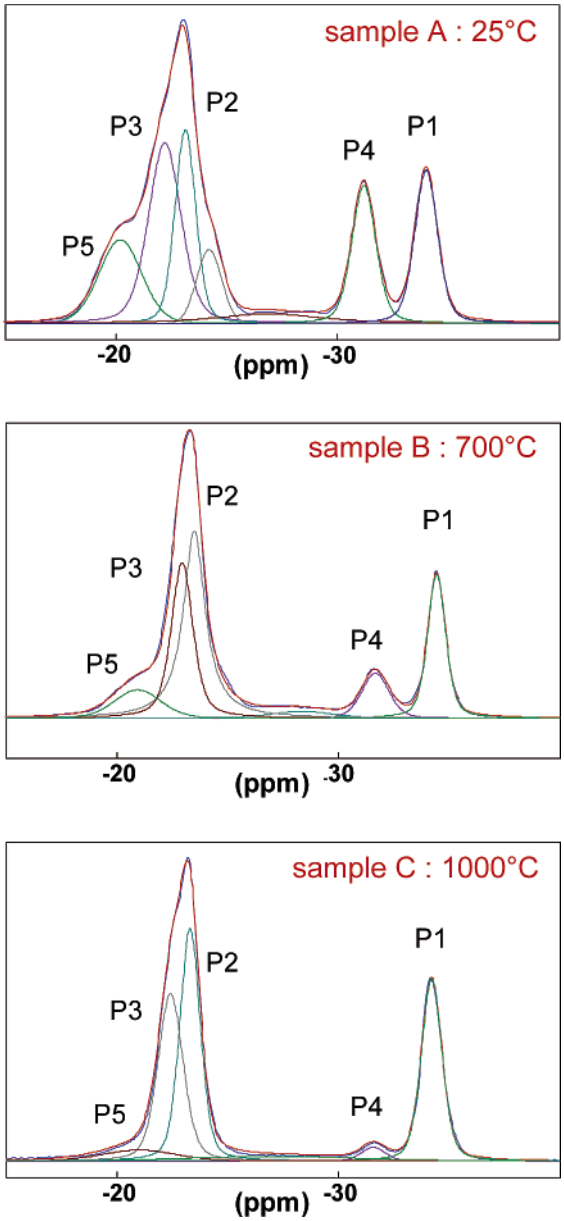

Figure 5. ^{31}P NMR MAS spectra of the three $La_{1/3}Zr_2(PO_4)_3$ samples: room temperature (sample A), quenched at 700 °C (sample B), and quenched at 1000 °C (sample C).

Table 5. Analysis of the ^{31}P NMR Mas Spectra of $La_{1/3}Zr_2(PO_4)_3$

	25 °C (A)			700 °C (quenched) (B)			1000 °C (quenched) (C)		
line	δ_{iso} (ppm) ±0.2	width (ppm) ±0.1	% ± 1	δ_{iso} (ppm) ±0.2	width (ppm) ±0.1	% ± 1	δ_{iso} (ppm) ±0.2	width (ppm) ±0.1	% ± 1
P(1)	−34.2	1.1	16	−34.4	1.0	19	−34.2	1.1	26
P(2)	−23.1	1.0	17	−23.4	1.2	36	−23.3	1.1	32
P(3)	−22.2	1.7	25	−22.8	1.1	25	−22.4	1.3	29
P(4)	−31.2	1.3	15	−31.7	1.4	8	−31.6	1.2	2
P(5)	−20.2	2.3	14	−20.9	2.5	9	−21.0	3.9	6

contrary to what has been observed with thermal X-ray diffraction. This may be due to the quenching process which was not sufficiently efficient. To fit the spectra at 25 and 700 °C, it was necessary to add two other contributions corresponding respectively to 13% of P content at 25 °C and 3% at 700 °C and which disappear at 1000 °C. This can be due to another kind of La^{3+} ordering in the $La_{1/3}Zr_2(PO_4)_3$ sample which was not visible on thermodiffraction patterns.

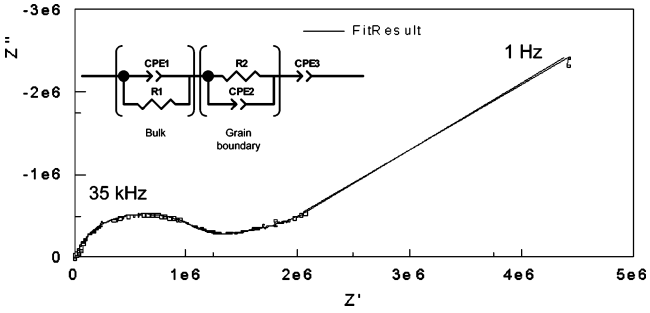

Figure 6. Complex impedance diagram in the Nyquist plane for $La_{1/3}Zr_2(PO_4)_3$ recorded in dry N_2 at 730 °C, with the equivalent electrical model used for experimental data fitting inserted.

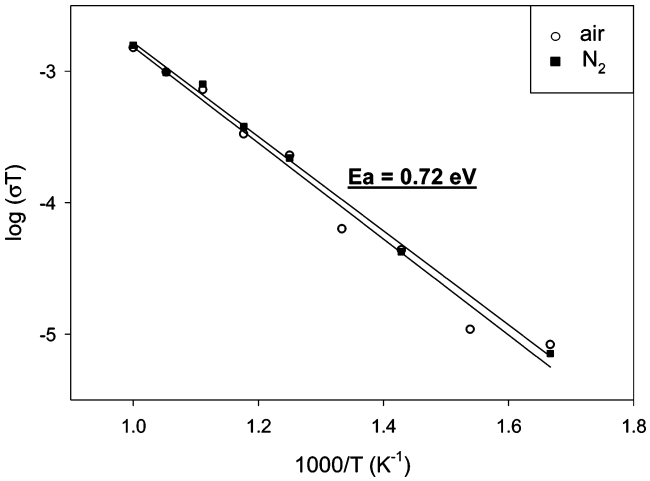

Figure 7. Logarithmic plot of ionic conductivity as a function of reciprocal temperature for $La_{1/3}Zr_2(PO_4)_3$.

Electrical Conductivity. The electrical properties of $La_{1/3}Zr_2(PO_4)_3$ have been investigated by means of impedance spectroscopy in the temperature range from 330 to 730 °C in air and in dehydrated N_2 atmospheres. No conductivity change between the two measurements series was observed, suggesting that the predominant conducting species is only ion and neither electron nor hole. Figure 6 shows a typical impedance plot, in the Nyquist plane obtained for $La_{1/3}Zr_2(PO_4)_3$ in dried N_2 at 730 °C. As expected, we observe a line at low frequency due to the electrode polarization (C = 10−1000 μF) which increases with temperature, confirming thus the ionic nature of the conductivity. At high frequency a semicircle is visible, the form of which indicates the presence of two different overlapping relaxation processes. Whatever the temperature, the data were refined with an equivalent electrical model (Figure 6) which represents the two relaxations and the electrode polarization. The dipolar part of our sample and the electrode polarization were modeled by a constant phase element (CPE), while the conductive part is represented by a resistance R. The two relaxations due to the ionic motion through the grain (bulk) and through the grain boundaries are separately refined but only the bulk conductivity is presented in this paper. At 600 °C, the bulk conductivity is $\sigma = 4.5 \times 10^{-7}$ S cm^{-1} in agreement with the values which were determined for other $RE_{1/3}Zr_2(PO_4)_3$ phases.[7,8] Figure 7 shows the temperature dependence of the La^{3+} ion conductivity plotted in an Arrhenius fashion. The deduced activation energy E_a = 0.72 eV is also very close

to those observed for this family compound published by Imanaka et al.[8,18]

Conclusion

The thermal study reveals that $La_{1/3}Zr_2(PO_4)_3$ exhibits at high temperature a structural transition from $P\bar{3}$ to $P\bar{3}c1$ induced by the La^{3+} ion ability to move in the $[Zr_2(PO_4)_3]^-$ network. Indeed, when the temperature is increased, the La3 site empties in favor of the La2 one. This structural modification is confirmed by ^{31}P NMR investigations which show the progressive disappearance of the P4 and P5 contributions. These peaks are linked to the presence of domains containing La^{3+} ion in the La3 site. In addition to these experiments, some conductivity measurements have been performed: the ionic conductivity ($\sigma = 4.5 \times 10^{-7}$ S cm^{-1} at 600 °C) is similar to the other $RE_{1/3}Zr_2(PO_4)_3$ published values.

(18) Imanaka, N.; Adachi, G. Y. *J. Alloys Compd.* **2002**, *344*, 137.

CM061610M